Effect of charge manipulation on scanning tunneling spectra of single Mn acceptors in InAs

Felix Marczinowski,* Jens Wiebe, Focko Meier, Katsushi Hashimoto,† and Roland Wiesendanger
Institut für Angewandte Physik, Universität Hamburg, Jungiusstrasse 11, D-20355 Hamburg, Germany
(Received 4 December 2007; published 13 March 2008)

We present scanning tunneling spectroscopy measurements on Mn-doped InAs at low temperatures. In the range of conduction band tunneling, we observe a ring of increased differential conductance around each individual Mn acceptor. With increasing bias voltage, the ring shrinks and finally collapses. When the ring crosses the acceptor, the well known asymmetric feature of the bound-hole wave function appears in topographs. The behavior is explained by the tip-induced decharging of the Mn, which influences the spectra outside the extension of the wave function. Using a simple model, we show that the ring shape is given by the equipotential lines of the tip-induced quantum dot, while its intensity allows us to measure the screened potential of the charged acceptor.

DOI: 10.1103/PhysRevB.77.115318 PACS number(s): 75.50.Pp, 71.55.Eq, 73.20.At, 73.20.Hb

Doping of III-V semiconductors with transition metal atoms can induce ferromagnetism, where the interaction between the local magnetic moments is mediated by itinerant holes.[1,2] It was shown by scanning tunneling microscopy (STM) that the hole state bound to a Mn acceptor in III-V's has a strongly anisotropic shape which is even more pronounced at surfaces,[3–5] leading to a highly anisotropic Mn-Mn interaction.[6] These facts explain the recent interest in the investigation of different dilute acceptors in III-V semiconductors by scanning tunneling spectroscopy (STS).[7–11]

The interpretation of STS results on semiconductors is complicated by the strong tip-induced band bending, which leads to a shift of the surface band structure with changing bias voltage. Since it is usually difficult to determine the work function of the tip exactly, a sufficiently precise Poisson calculation is often not feasible. This has led to contradicting interpretations of the origin of the anisotropic shape of acceptor features in STM/STS data.[3,5,8,10] While the anisotropic feature from Mn acceptors in GaAs and InAs was interpreted as a direct image of the bound-hole wave function,[3,5] the results on Zn and C acceptors in GaAs imply that this shape is induced by the asymmetry of evanescent gap states.[10] In the latter experiments, the local dI/dz was used to determine the tip work function and thus to calculate the tip-induced band bending.

An independent method to determine the tip-induced band bending is described in this STM/STS study of Mn acceptors in InAs. We find rings of increased differential conductance around each Mn, which shrink in size for increasing bias voltage and finally collapse. A similar effect has been observed for a doped layer of C_{60} molecules on thin insulating layers,[12,13] chargeable grains on semiconductors,[14,15] and different impurities in semiconductors.[16–18] The latter employ an advanced nonequilibrium theory including a switching charge, without specifying its exact location. Using a simple model, we show that the ring can be interpreted as the impact of the tip-induced Mn decharging process on the conduction band tunneling, which allows us to determine the bias voltage at which the acceptor level is pushed above the bulk Fermi energy E_F. Since the well known anisotropic Mn feature appears in topographs at exactly this voltage, its interpretation as a direct image of the bound-hole wave function is substantiated.[5] The rings furthermore allow to determine the shape of the tip-induced band bending as well as to measure the decay of the screened potential of the charged Mn.

I. EXPERIMENTAL PROCEDURES

The measurements were conducted in two ultrahigh-vacuum (UHV) STM systems, at a temperature of 6 K (Ref. 19) and at 4 K.[20] Both systems have base pressures below $p=1\times10^{-10}$ mbar. We used polycrystalline tungsten tips made by electrochemical etching, which were prepared for measurement by flashing to 1800–2300 K under UHV conditions.[5,20] Our samples were commercially produced Mn-doped InAs single crystals with doping concentrations of 1×10^{17} and 1×10^{19} cm^{-3}, which are paramagnetic at our measurement temperature, as confirmed by superconducting quantum interference device (SQUID) measurements. Since these Mn densities are well below the solubility limit, the samples are virtually free of unwanted defects such as interstitial Mn or MnAs clusters, otherwise found in highly Mn-doped samples. The crystals were cleaved at room temperature under UHV condition along the (110) plane, resulting in an almost defect-free surface.[21] For topographic measurements, the STM was operated in constant-current mode with the voltage U applied to the sample with respect to the tip. In order to acquire spectroscopic information, a small ac signal (called modulation voltage, U_{mod}) is added to U, allowing to measure the local differential conductance (dI/dU) by means of lock-in technique. This can be done simultaneously to constant-current images in order to acquire a map of the differential conductance of the imaged surface area, a so-called dI/dU map, at the corresponding U. To obtain dI/dU information over a full range of voltages [$dI/dU(U)$], the STM tip is first stabilized with the feedback circuit at a stabilization voltage U_{stab} and current I_{stab} and then held fixed, while a voltage ramp through the desired range is performed and the dI/dU signal is recorded. This way, the dI/dU spectrum for a single point of the sample is obtained (single point spectrum). If this is done for every point on a grid spanning a certain surface area, a spectroscopic field $dI/dU(U,x,y)$ for this area is obtained. By evaluating a slice of a spectroscopic field at a certain U, again a spatial map of the dI/dU signal can be created, a so-called dI/dU slice. Different ways

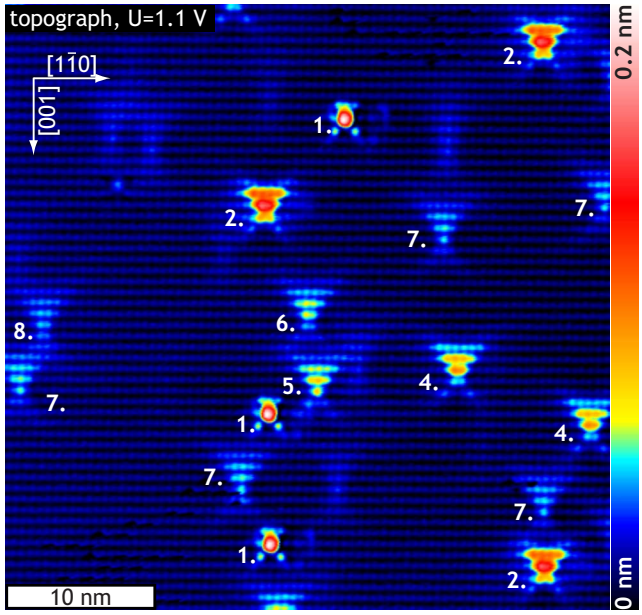

FIG. 1. (Color online) STM topograph of the (110) surface of Mn-doped InAs (U=1.1 V, I_{set}=0.5 nA, and $n \approx 1 \times 10^{19}$ cm^{-3}). Mn dopants in different depths below the surface (as annotated) are visible as asymmetric crosslike protrusions. The As atoms of the host lattice are visible as a regular pattern.

of spatially averaging spectra from spectroscopic fields were employed. We emphasize that the $dI/dU(U)$ spectra shown in this work cannot be interpreted directly as the local density of states (LDOS) at the corresponding energy eU, as done in most STS works. The reason is the strong tip-induced band bending,[22,23] which has to be taken into account.

II. EXPERIMENTAL OBSERVATIONS

A typical STM topograph of the highly doped (1×10^{19} cm^{-3}) sample taken at moderate positive bias voltage ($\sim$1 V), is shown in Fig. 1. The most obvious features are protrusions with highly anisotropic and asymmetric shape, caused by Mn acceptors in different (110) planes below the surface.[5] Additionally, the atomic lattice of the As atoms in the surface can be seen clearly.

The absolute depth of the dopant below the surface can be determined up to the eighth layer in most cases. The apparent height of the Mn feature decreases monotonically with increasing depth, with the exception of acceptors in the surface layer, which appear 40% lower than those one layer deep.[5] Furthermore, the topographic feature is found either centered on the [001] As rows or centered in between two rows. This defines the parity of the layer containing the acceptor, reducing uncertainties in the apparent height. The depth of each dopant determined this way is given in Fig. 1. Note that the numbering starts at zero; thus, the surface layer is called the zeroth layer. Acceptors deeper than eight to ten layers are still clearly visible, but their depth cannot be determined without ambiguity, and we therefore omit the numbering for

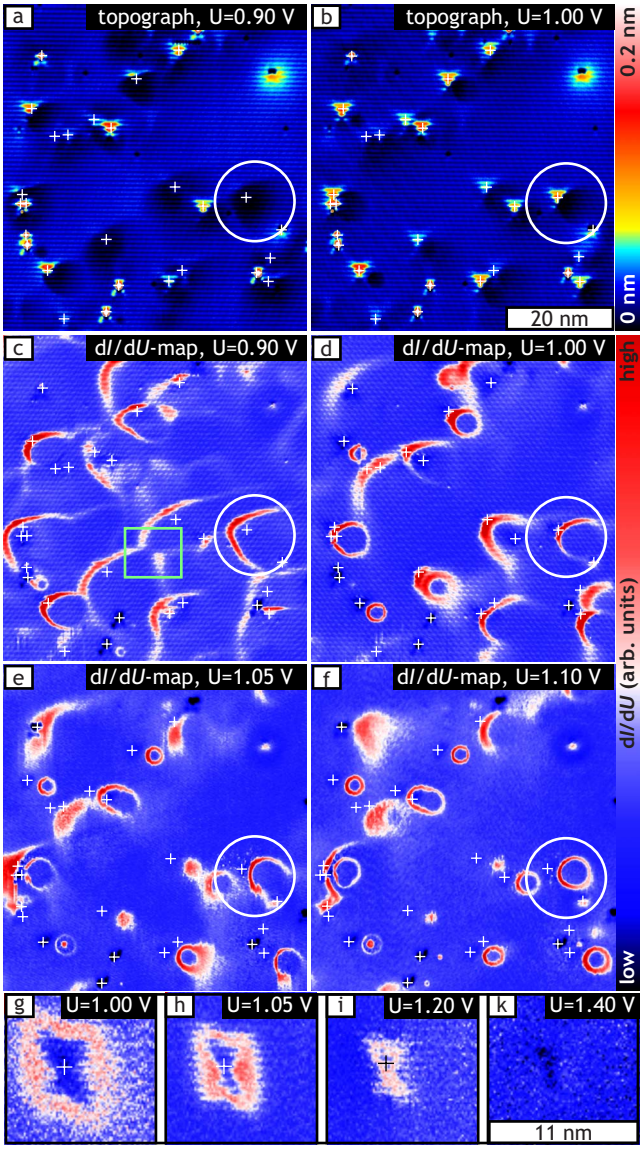

FIG. 2. (Color online) Evolution of the ringlike feature in dI/dU maps over voltage. [(a) and (b)] STM topographs obtained at U as indicated, I_{set}=0.5 nA. [(c)–(f)] dI/dU maps of the same area with increasing U (U_{mod}=10 mV and $n \approx 1 \times 10^{19}$ cm^{-3}). The center of the evolving feature is slightly shifted away from the dopant positions, which are marked with white crosses. This can, for example, be seen in the evolution of the ring from one dopant, marked by white circles in (c)–(f). In (c), note the "anticrossing" marked by a green square. [(g)–(k)] demonstrates the short range evolution of the feature in a series of dI/dU slices (U_{stab}=1.5 V, I_{stab}=0.6 nA, and U_{mod}=10 mV, U as indicated) measured with a differently shaped tip on a lower doped sample $n \approx 1 \times 10^{17}$ cm^{-3}.

those Mn dopants. The observed anisotropic Mn features are interpreted as direct images of the highly anisotropic bound-hole wave function as shown by comparison to tight-binding calculations. The strong asymmetry of the acceptor state close to the surface is caused by (not acceptor related) lattice deformations due to surface relaxation.[5]

Figures 2(a) and 2(b) show two STM topographs, both acquired from the same sample area at slightly lower bias

voltages than in Fig. 1. The positions of the Mn acceptors in different depths, as obtained from topographs at higher voltage, are marked by white crosses. Obviously, some of the Mn acceptors are not imaged at $U=0.9$ V in Fig. 2(a). Instead, a faint larger scale depression is observed around or close to those acceptors. This depression becomes smaller at higher bias voltage and the previously invisible anisotropic feature appears [compare white circles in Figs. 2(a) and 2(b)]. At even higher bias voltages, the depression in STM topographs completely vanishes, leaving behind just the anisotropic Mn features as in Fig. 1. Due to this bias dependency of the large scale depression, we conclude that it is of purely electronic origin. Figures 2(c)–2(f) show the dI/dU maps acquired simultaneously to the topographs with increasing bias voltage. The images show zones of enhanced differential conductance (in red) on a background of lower signal (blue). Corresponding to the depression in topographs, we find around each Mn acceptor a bow or ringlike feature of increased differential conductance, tracing the sharp borders of the topographic depression. The feature appears as a faint extended bow like the one marked by the white circle in Fig. 2(c). With increasing voltage, the feature shrinks toward its central point [see white circles in (d) and (e)]. Exactly when the ring crosses the position of the corresponding Mn acceptor, the asymmetric LDOS of the Mn-acceptor wave function appears in topography [see circles in (b) and (d)]. At even higher voltage, each bow eventually closes and forms a ring, as marked by the circle in (f). This ring continues to shrink for further increased voltages and finally forms a bright spot slightly beside the location of an acceptor, before it vanishes completely.

Each of the described ring features develops in a similar fashion, although not exactly identical as they overlap and seem to interact [see, for example, the area marked by a square in (c)]. Each ring is clearly related to a Mn acceptor close to its center. The bias voltage at which the ring appears depends on the local environment of the acceptor and is spread over a range of about 0.3 V.

In experiments with different STM tips, a strong influence of the tip shape and material on the described topographic depression and dI/dU rings is observed. As an example, panels (g)–(k) of Fig. 2 show dI/dU slices from an STS measurement of a single acceptor in a lower doped sample, using a different tip than in (a)–(f). Due to the low doping, no interaction effects are observed. With this particular tip, the dI/dU ring appeared to be centered perfectly around the position of the Mn acceptor marked by a cross. The shape of the ring immediately before it collapses, as shown in Figs. 2(g) and 2(h), has the symmetry of the Mn-acceptor wave function. In Fig. 2(i), the ring closes and perfectly resembles the shape of the acceptor wave function as calculated in a tight-binding model.[5] Finally, in (k), the ring has disappeared and only a small-scale depression about the size of the acceptor is left.

We assume that the apex of this particular tip was very symmetric, leading to the high symmetry of the observed ring feature in relation to the Mn-acceptor position. The tip used for the images in Figs. 2(c)–2(f), however, was much more asymmetric, with the foremost imaging tip atom aside from the symmetry center of the tip. As a consequence, the ring centers are located aside from the topographic Mn feature in Figs. 2(c)–2(f).

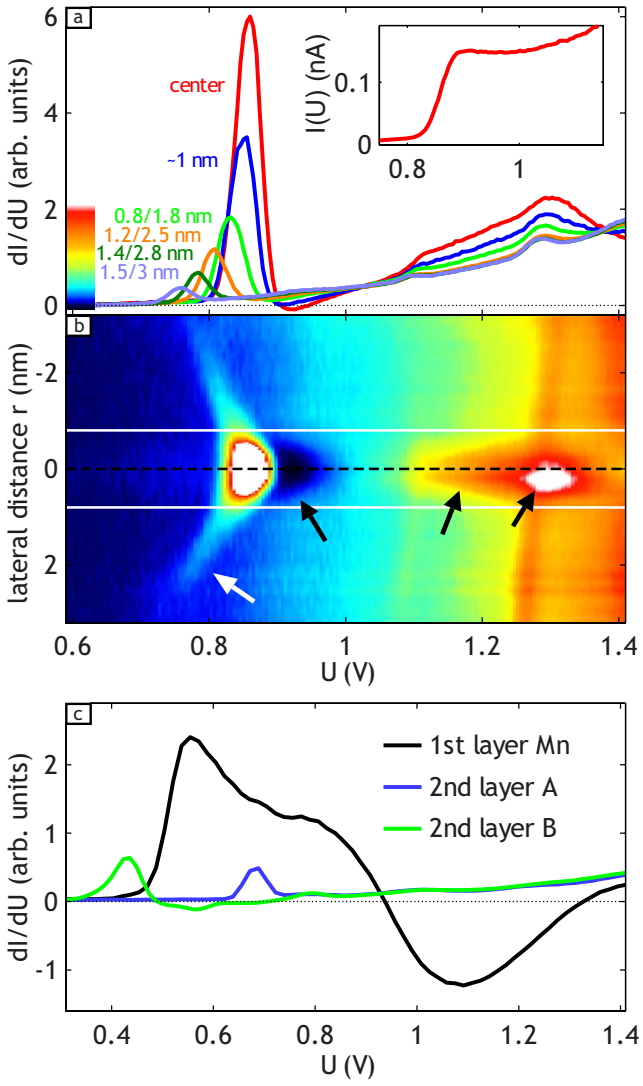

FIG. 3. (Color online) (a) dI/dU spectra averaged over the ring feature for different ring diameters, as indicated. Since the ring is not circular, the numbers give the minimum and maximum distances to the Mn center. The small inset graph shows the $I(U)$ curve corresponding to the dI/dU curve labeled "center" (red). (b) Color-coded dI/dU spectra measured in different lateral distances from the Mn center, as indicated by the y axis. The mapping of energy to color is given by the color bar in (a). The two horizontal white lines and the dotted black line indicate the extension of the acceptor state and its center in the topograph. The bow like feature (white arrow) is equivalent to the ring feature in dI/dU maps. The localized nature of the observed NDC (black area) as well as of the follow-up peaks are visible (see black arrows) ($U_{\mathrm{stab}}=2$ V, $I_{\mathrm{stab}}=2$ nA, and $U_{\mathrm{mod}}=20$ mV; (c) dI/dU spectra on two second layer Mn (A and B) and a first layer Mn showing strong NDC ($U_{\mathrm{stab}}=1.8$ V, $I_{\mathrm{stab}}=1$ nA, $U_{\mathrm{mod}}=20$ mV, and $n\approx 1\times 10^{19}$ cm^{-3}).

When performing STS on the center of the (topographic) Mn feature of a Mn atom in the second layer, a dI/dU spectrum, as shown in Fig. 3(a), is obtained. The pronounced peak at ~0.85 V corresponds to the situation shown in

Fig. 2(i) and marked by the circle in Fig. 2(d), where the dI/dU ring crosses the Mn position and the anisotropic Mn feature appears in topography. A spectrum averaged over the ring at a lower voltage (and thus at a larger distance from the Mn center) is also shown in Fig. 3(a) (in blue), where a relatively smaller peak is observed. This peak is the dI/dU intensity forming the ring feature in dI/dU maps, and so appears at lower energies for increasing lateral distance from the Mn center (additional curves). The ranges given for the lateral distance are a result of the feature's noncircular shape of the ring. Furthermore, we observe negative differential conductance (NDC) at the center of the Mn acceptor, as shown in the inset of Figs. 3(a) and 3(c). This NDC is only found for some ($\approx 1/3$) of our tips and is strongest on dopants one layer below the surface [see Fig. 3(c)]. It is much weaker for dopants in the second layer and hardly observable for those in the third layer. We also regularly observe follow-up peaks above the main peak, i.e., in Fig. 3(a) at 1.1 and 1.3 V, which were assigned to the spin-orbit split states of the acceptor.[5] We would also like to point out that the main peak often has a pronounced shoulder for the acceptors in the first layer as visible in Fig. 3(c).

Figure 3(b) gives a different view of the same spectroscopic data set as in (a). The dI/dU intensity is color coded, and the y axis gives the real-space displacement along a line through the center of a Mn acceptor. The dotted line indicates the position of the Mn. The ring feature, which in Fig. 3(a) took the form of a series of peaks, now shows up as two "wings" (indicated by a white arrow) beside the main central peak, extending far out from the acceptor. A possible explanation for the vertical red stripe around 1.3 V is that it is the ring feature of another more distant Mn acceptor. In strong contrast to this, the main peak, the NDC, and the follow-up peaks (black arrows) are strictly confined to a range of less than 1 nm from the center, i.e., few surface unit cells wide. Therefore, we attribute the local phenomena to effects of the Mn-acceptor LDOS, as discussed in our earlier publication,[5] while the extended ring feature needs a different explanation which we deal with in the next section.

III. INTERPRETATION

As our samples had a rather low carrier density, band-bending effects will play a major role and must be taken into account. The difference in work functions of the used W tips and InAs plus the applied sample bias leads to band bending at the sample surface in the vicinity of the STM tip. This effectively shifts the LDOS $\rho_S(E)$ of the sample with regard to the tip by some amount $\phi_{\mathrm{BB}}(U)$ that can be included in the canonical equation for the tunneling current in the Tersoff–Hamann model,[24,25]

$$I(U) \propto \int_{E_F}^{E_F+eU} \rho_S(\epsilon + \phi_{\mathrm{BB}}(U))\rho_T(\epsilon - eU)T(\epsilon, U, z)d\epsilon, \tag{1}$$

with the tip density of states ρ_T and the transmission coefficient $T(\epsilon, U, z)$. As a consequence, at least a rough understanding of the extent and amount of the band bending must exist prior to any solid interpretation of the STS spectra. To achieve this, we used a Poisson solver specialized for a one-dimensional model of an STM tunnel junction on a semiconductor sample.[26] The calculated band profiles for three different bias voltages are shown in the left panels of Fig. 4. For this calculation, we used the tip work function $\Phi_{\mathrm{tip}}=4.5$eV, the electron affinity of the sample $E_A=4.9$eV, the acceptor energy $E_{\mathrm{acc}}=28$ meV and acceptor concentration 1×10^{19} cm^{-3}, the band gap $E_{\mathrm{gap}}=0.41$ eV, and the tip-surface distance of $z=6$ Å. Note that the energy separation of the acceptor level with regard to the valence band has been exaggerated in the pictures. We did not calculate the lateral extension of the space-charge region which will depend crucially on the exact shape of the STM tip. The right panels of Fig. 4 show instead a sketch of the lateral profile of the band bending as a function of the distance r from the base of the center of the tip.

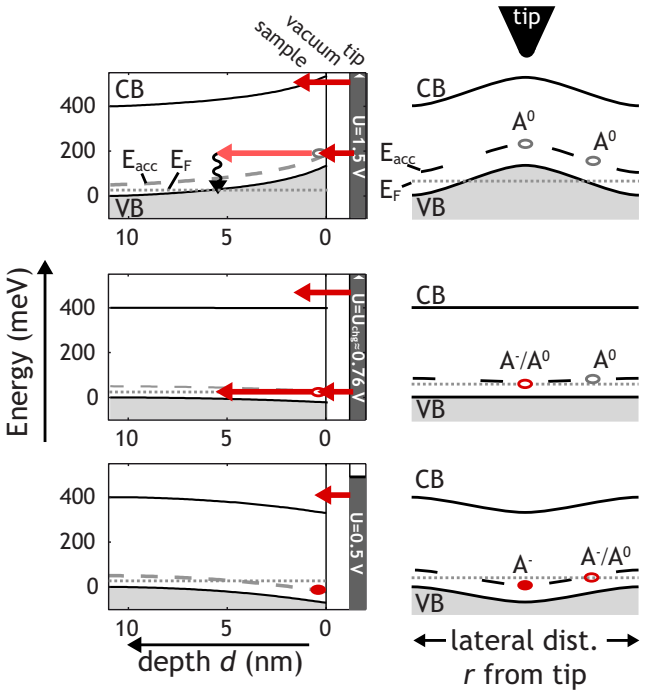

FIG. 4. (Color online) Band bending below the STM tip for different bias voltages. Left column: Depth-dependent band bending of valence band (VB), conduction band (CB), and acceptor level (E_{acc}) towards surface below the STM tip position. The energy of the acceptor level with regard to the VB is exaggerated for clarity. Shown are numerically obtained solutions of the one dimensional Poisson equation. The dotted line indicates the bulk Fermi energy (E_F). Right column: Schematic lateral run of sample energy bands below the STM tip. Charged (neutral) acceptors are indicated with A^- (A^0). A^-/A^0 denotes an acceptor which is at E_F.

The bands become flat when U equals $U_{\mathrm{FB}}=(E_A+E_{\mathrm{gap}}-E_{\mathrm{acc}}/2-\Phi_{\mathrm{tip}})/e=0.8$ V. At a slightly lower bias voltage U_{charge}, shown in the middle panels of Fig. 4, an acceptor right below the STM tip (A^-/A^0, red ellipse) is "in resonance" with the bulk Fermi level E_F and the DOS provided by the impurity band and/or valence band edge. This leaves an open tunneling path for electrons from the tip via the

acceptor into the bulk of the sample along E_F (see arrows). At the same time, the tip Fermi level is already overlapping with the conduction band, which gives its own contribution to the tunneling current (upper arrow). An acceptor that is laterally some distance apart from the tip will have its acceptor state slightly above E_F and therefore uncharged (gray ellipse in middle right panel, A^0).

For $U < U_{\text{charge}}$, the negatively charged acceptors A^- make up the screening charge density (bottom panels of Fig. 4). Their low density leads to an extended and smooth bending of the DOS bands, reaching ≈ 10 nm into the sample for $U = 0.5$ V. In this space-charge region, E_F lies in the band gap above the impurity band or even in the (bent down) conduction band if $U < -0.3$ V. The only conductivity is provided by the bulk bands, either from occupied tip states to the conduction band or ($U < 0$ V) from valence band states to unoccupied tip states. Since the screening potential in the sample decays laterally, the impurity band crosses E_F at some finite distance (bottom right). For $U > U_{\text{charge}}$, on the other hand, the acceptor level is raised out of resonance, above E_F, on a small scale. For an electron to move via a surface acceptor to the back contact of the sample, it needs to loose energy, e.g., to a phonon. At low temperatures, this relaxation might be inhibited due to the lack of phonons. Consequently, the conductance path created by emptying the acceptor at U_{charge} might be suppressed again at higher bias voltages.

The creation of the additional tunneling path through the acceptor with increasing voltage will lead to an increase of the current, i.e., a peak in the dI/dU signal. When this is followed by the suppression of the same channel with increasing bias voltage, the current contribution vanishes again, and instead of a step, a peak is observed in $I(U)$, and accordingly the peak in dI/dU is followed by a dip with negative dI/dU. This matches our measurements showing a peak and NDC obtained at the center of surface-near Mn acceptors, as shown in Fig. 3(a). Since the described process involves directly tunneling into the (localized) acceptor state, it will be confined to a small surface area, where this state overlaps with tip states. The confinement of the strong peak and NDC structure to roughly 1.5–2 nm matches the size of the acceptor wave function, as obtained from a tight-binding model.[5] Since two effects are combined here, tunneling via the (p-like) acceptor state and tunneling into the (s-like) conduction band onset, a preference of the tip for certain states (s-like, p-like) might sufficiently explain why NDC is not observed with all tips.

The observed ring structure in dI/dU maps, however, cannot be explained by the presence of the acceptor wave function. This dI/dU peak forming the aforementioned ring feature is observed much farther away from the Mn center (up to 20 nm) than the Mn-acceptor wave function. The source of this distance dependent peak becomes apparent when the effect of the charge change of the acceptor on a dI/dU measurement is taken into account. As shown in the bottom right panel of Fig. 4, a sufficiently strong downward band bending by the tip potential will cause an acceptor level to cross E_F in some lateral distance r from the tip (A^-/A^0). With a bias voltage of U_{charge}, only acceptors directly below the tip lie at E_F. Going down in voltage, the downward band bending becomes stronger and the crossing radius becomes larger. An acceptor outside this radius is above E_F and uncharged (A^0), while inside the radius, it lies below E_F and thus is in the charged configuration (A^-). From the point of view of an isolated acceptor, there is a radius inside which the STM tip lowers the local potential sufficiently to switch it into the charged state. If the tip is outside this radius, the acceptor is neutral. If in an STS measurement the voltage ramp causes the switching radius to extend across this acceptor, it will become charged, resulting in a peak in dI/dU, as will be explained in the next section. In other words, the rings are caused by the switching of a charge some nanometers away from the tip base point.

The coincidence of the dI/dU ring with the Mn-acceptor position thus marks the voltage at which the acceptor becomes neutral. At this voltage and above, we observe the anisotropic crosslike feature in STM topographs [compare circles in Figs. 2(b) and 2(d)]. Therefore, we conclude that this crosslike feature is indeed induced by the LDOS of the acceptor; more precisely, it is a direct image of the acceptor wave function, as stated previously.[5] This interpretation differs from the results on Zn and C impurities in GaAs, where similar anisotropic feature and NDC were explained by resonant tunneling through evanescent gap states.[10]

Effect of charging on dI/dU spectra

The following section describes a simple model to understand the effect of charging on the dI/dU spectra. When charging the acceptor, the abrupt change in the local potential has an effect on the surrounding of the acceptor, fading with distance due to screening effects. In other words, the acceptor contributes to its environment an additional spatially varying offset potential $\phi_{\text{charge}}(r,U)$ corresponding to its charge state and thus dependent on U. It is important to mind now that in the considered voltage range (about 0.4 V–0.9 V), basically only conduction band states are involved in the tunneling process, as long as tip states are not directly overlapping with an acceptor state. Going from lower voltages upward in a spectroscopy measurement with fixed tip or, equivalently, entering the switching radius of an acceptor at a fixed bias voltage, the local potential will abruptly jump downward as the acceptor goes from A^- to A^0. The effect of this process on the tunneling current can still be understood within the Tersoff–Hamann model.[24] In a very straightforward manner, we can consider this changing potential in the form of an additional offset to $\epsilon + \phi_{\text{BB}}(U)$ in the argument of the sample LDOS ρ_S in Eq. (1). As a consequence, above the switching point, the sample LDOS in the current integral gets shifted down in energy, yielding a higher current than below the switching point. This step up in current or peak in dI/dU matches our observations in Fig. 3. Since this is no separate Mn-related tunneling mechanism but solely an effect of the interaction between the tip potential, the acceptor charge, and the LDOS below the tip, the extended range of the effect is plausible.

This very simple model is able to reproduce the discussed peak and ring feature qualitatively with remarkable accuracy, as shown in Fig. 5. For this calculation, we used a simple

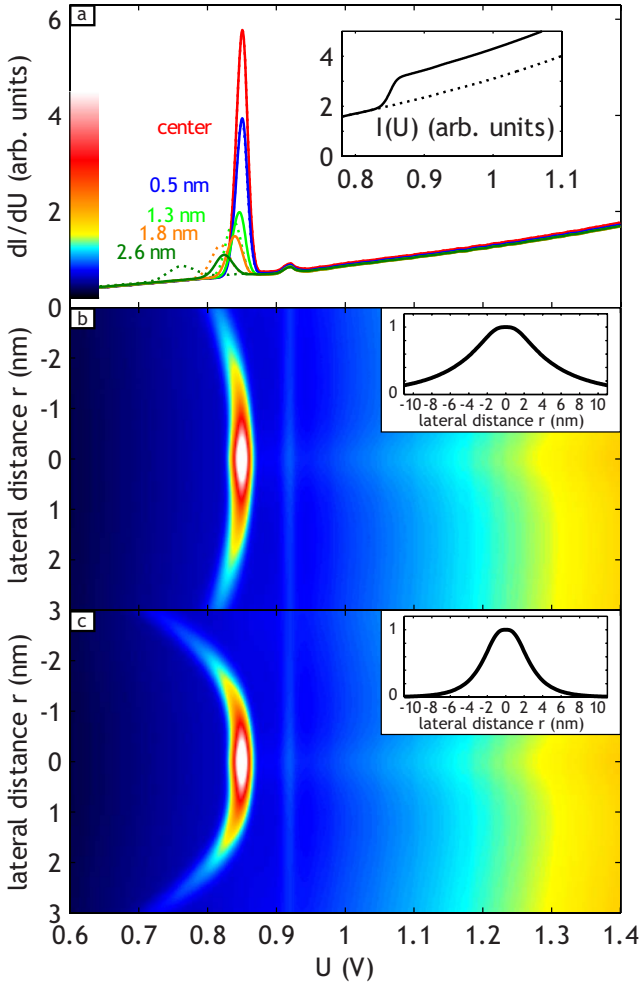

FIG. 5. (Color online) Model of charge-switching effect in dI/dU spectra (see text for details). (a) Simulated dI/dU spectra in the presence of a switchable charge calculated for two different tip potential diameters ($D_{\mathrm{FWHM}}=10$ nm, solid line; $D_{\mathrm{FWHM}}=5$ nm, dashed line) and tip-charge distances as indicated. Inset: Simulated current vs voltage for central spectrum. The dotted line shows the current without influence of a charge. (b) and (c) show color-coded spectra calculated at different lateral distances r from the charge center for the wider tip (10 nm) and for the narrower tip (5 nm), respectively. The insets show the lateral profile of the tip potential within the sample.

form of the current in the Tersoff–Hamann model assuming constant tip density of states,

$$I(U) = \int_{E_F}^{E_F+eU} \rho_S\big(\epsilon + \phi_{\mathrm{BB}}(U)\big) T(\epsilon, U, z) d\epsilon, \tag{2}$$

$$\rho_S(E) = \begin{cases} \sqrt{E - E_{\mathrm{CB}}} & \text{for } E > E_{\mathrm{CB}} \\ 0 & \text{for } E \leqslant E_{\mathrm{CB}}, \end{cases} \tag{3}$$

$$T(\epsilon, U, z) = \exp\left[-2z \sqrt{\frac{2m_e}{\hbar^2}(\bar{\Phi} + eU/2 - \epsilon)} \right], \tag{4}$$

$$\bar{\Phi} = (\Phi_{\mathrm{tip}} + \Phi_{\mathrm{sample}})/2. \tag{5}$$

We further assumed that the tip causes a voltage dependent band bending $\phi_{\mathrm{BB}}(U,r)$ as simulated by the aforementioned Poisson solver, which decays laterally with r analogous to the case of a hyperbolic tip.[27] The used decay functions for two different tip diameters are also shown in the inset graphs in Figs. 5(b) and 5(c). We then assumed the acceptor's localized charge in a given total distance $r_{\mathrm{acc}}=\sqrt{r^2+{d_{\mathrm{acc}}}^2}$ (d_{acc}, acceptor's depth below surface) from the tip base point to switch if $\phi_{\mathrm{BB}}(U,r)=-E_{\mathrm{acc}}/2=14$ mV, i.e., when the local band bending aligns the acceptor state with E_F. For numerical stability and as a crude simulation of thermal and other broadening effects, we simulated the switching as a soft transition broadened by 1 meV. We assumed the potential of the localized charge to decay like[28]

$$\phi_{\mathrm{charge}}(r_{\mathrm{acc}}) = \frac{e}{4\pi\epsilon\epsilon_0 r_{\mathrm{acc}}} e^{-r_{\mathrm{acc}}/r_{\mathrm{screen}}}, \tag{6}$$

with $\epsilon=14.6$ and $d_{\mathrm{acc}}=0.43$ nm$=2$ ML depth of the acceptor.

A resulting $I(U)$ curve as well as derived dI/dU curves are given in Fig. 5(a). Using the screening length r_{screen}, the tip work function Φ_{tip}, and the extension of the tip potential D_{FWHM} as the only free parameters, we achieved the best agreement with the data shown in Fig. 3 for $r_{\mathrm{screen}}=10$ nm, $\Phi_{\mathrm{tip}}=4.38$ eV (theoretically 4.5 eV), and $D_{\mathrm{FWHM}}=5-10$ nm. The peculiar shifting and lowering of the peak observed in the measurements are excellently reproduced by the model. A notable difference between experimental and simulated results is found around $r=0$ nm: the NDC as well as a brighter central peak and the follow-up peaks are missing in the simulation. As stated above, we attribute the localized peak and NDC structure and the follow-up peaks to direct tunneling via the localized acceptor LDOS, which is not modeled here but was described in an earlier publication.[5]

The specific shape of the observed ring features can now be interpreted as the signature of the lateral tip-induced band-bending profile for different bias voltages. The observed rings can be understood as equipotential lines of the tip, as seen by the acceptor. This shape will only be circular for very regular tips and smooth acceptor potentials. Only such tips will accurately reproduce the local symmetry of the Mn wave function in dI/dU maps like in Figs. 2(g)–2(k). The observed noncircular profiles as well as profiles having their center beside the Mn position [Figs. 2(c)–2(f)] are due to tips which were irregularly shaped at the very end. Moreover, the bias voltage at which the ring crosses the Mn acceptor can be unambiguously assigned to the voltage U_{charge} at which the acceptor is pushed above E_F without exact knowledge of the tip work function. Note that U_{charge} is different from the bias voltage U_{FB} (which induces flat bands) by several tens of meV, due to the binding energy of the acceptor E_{acc}. Furthermore, E_{acc} can differ from the bulk value due to the confinement effect of the tip-induced band bending. Our model additionally shows that the strength of the peak in the dI/dU signal belonging to the ring can be taken as a quantitative measure for the strength of the accep-

tor potential at the tip base point. The distance-dependent decay of the peak thus allows us to gauge the screening behavior for acceptor charges.

SUMMARY

We observed a complex spectroscopic feature set on Mn acceptors in InAs: (i) conduction band related rings with increased dI/dU and peak energies shifting coherently with distance from the acceptor and (ii) a combination of peak and NDC localized on the Mn acceptor. Comparison with a simple model in a Tersoff–Hamann picture, taking into account the tip-induced band bending, reveals that (i) can be fully explained by the tip-induced quantum dot, which decharges individual acceptors with increasing bias voltage and thereby influences the conduction band LDOS at the tip position. This allows us to unambiguously assign the voltage U_{charge} at which the acceptor gets neutral. The appearance of the well known anisotropic topographic signature of the acceptor exactly at U_{charge} substantiates its interpretation as a direct image of the bound-hole acceptor wave function. Furthermore, the rings can be interpreted as equipotential lines of the tip-induced quantum dot, while their intensity allows us to directly measure the decay of the screened Coulomb potential of the charged acceptor. However, the interpretation of ring shape and intensity has to be taken with care for smaller Mn-Mn distances that cause strong Coulomb interactions. In this case, the rings will interact, as marked by the square in Fig. 2(c). The detailed analysis of such crossings can be used to study the interaction between individual acceptors which is beyond the scope of the present work.

ACKNOWLEDGMENTS

We thank P. M. Koenraad, S. Loth, and M. Wenderoth for helpful discussions and for providing the Poisson solver. We thank O. Albrecht and D. Görlitz for the SQUID measurements. We acknowledge financial support from the *Deutsche Forschungsgemeinschaft* within SFB 508 "Quantum Materials" and *Graduiertenkolleg 1286* "Functional Metal-Semiconductor Hybrid Systems."

*marczinowski@physnet.uni-hamburg.de;
http://www.nanoscience.de/group_r/
†Present address: Solid-State Quantum Transport Group, Department of Physics, Tohoku University, Sendai 980-8578 Japan.

[1] H. Ohno, H. Munekata, T. Penney, S. von Molnár, and L. L. Chang, Phys. Rev. Lett. **68**, 2664 (1992).
[2] H. Ohno, A. Shen, F. Matsukara, A. Oiwa, A. Endo, S. Katsumoto, and Y. Iye, Appl. Phys. Lett. **69**, 363 (1996).
[3] A. M. Yakunin, A. Y. Silov, P. M. Koenraad, J. H. Wolter, W. Roy, J. D. Boeck, J.-M. Tang, and M. E. Flatté, Phys. Rev. Lett. **92**, 216806 (2004).
[4] A. M. Yakunin *et al.*, Nat. Mater. **6**, 512 (2007).
[5] F. Marczinowski, J. Wiebe, J.-M. Tang, M. E. Flatté, F. Meier, M. Morgenstern, and R. Wiesendanger, Phys. Rev. Lett. **99**, 157202 (2007).
[6] D. Kitchen, A. Richardella, J.-M. Tang, M. E. Flatté, and A. Yazdani, Nature (London) **442**, 436 (2006).
[7] P. I. Arseev, N. S. Maslova, V. I. Panov, S. V. Savinov, and C. Van Haesendonck, JETP Lett. **77**, 172 (2003).
[8] G. Mahieu, B. Grandidier, D. Deresmes, J. P. Nys, D. Stiévenard, and P. Ebert, Phys. Rev. Lett. **94**, 026407 (2005).
[9] S. Loth, M. Wenderoth, L. Winking, R. G. Ulbrich, S. Malzer, and G. H. Döhler, Jpn. J. Appl. Phys., Part 1 **45**, 2193 (2006).
[10] S. Loth, M. Wenderoth, L. Winking, R. G. Ulbrich, S. Malzer, and G. H. Döhler, Phys. Rev. Lett. **96**, 066403 (2006).
[11] D. Kitchen, A. Richardella, P. Roushan, J.-M. Tang, M. E. Flatté, and A. Yazdani, J. Appl. Phys. **101**, 09G515 (2007).
[12] N. A. Pradhan, N. Liu, C. Silien, and W. Ho, Phys. Rev. Lett. **94**, 076801 (2005).
[13] G. V. Nazin, X. H. Qiu, and W. Ho, Phys. Rev. Lett. **95**, 166103 (2005).
[14] J. W. G. Wildöer, A. J. A. van Roij, C. J. P. M. Harmans, and H. van Kempen, Phys. Rev. B **53**, 10695 (1996).
[15] N. Maslova, S. Oreshkin, V. Panov, S. Savinov, A. Depuydt, and C. Van Haesendonck, JETP Lett. **67**, 146 (1998).
[16] P. Arseev, N. Maslova, and S. Savinov, JETP Lett. **68**, 320 (1998).
[17] A. Depuydt, C. Van Haesendonck, N. S. Maslova, V. I. Panov, S. V. Savinov, and P. I. Arseev, Phys. Rev. B **60**, 2619 (1999).
[18] N. S. Maslova, S. I. Oreshkin, V. I. Panov, and S. V. Savinov, *Proceedings of the Eight International Symposium on Nanostructures: Physics and Technology, St. Petersburg, Russia, 19–23 June 2000* (Ioffe Institute, St. Petersburg, Russia, 2000).
[19] C. Wittneven, R. Dombrowski, S. H. Pan, and R. Wiesendanger, Rev. Sci. Instrum. **68**, 3806 (1997).
[20] J. Wiebe, A. Wachowiak, F. Meier, D. Haude, T. Foster, M. Morgenstern, and R. Wiesendanger, Rev. Sci. Instrum. **75**, 4871 (2004).
[21] J. Klijn, L. Sacharow, C. Meyer, S. Blügel, M. Morgenstern, and R. Wiesendanger, Phys. Rev. B **68**, 205327 (2003).
[22] R. Dombrowski, C. Steinebach, C. Wittneven, M. Morgenstern, and R. Wiesendanger, Phys. Rev. B **59**, 8043 (1999).
[23] G. J. de Raad, D. M. Bruls, P. M. Koenraad, and J. H. Wolter, Phys. Rev. B **66**, 195306 (2002).
[24] J. Tersoff and D. R. Hamann, Phys. Rev. B **31**, 805 (1985).
[25] R. Wiesendanger, *Scanning Probe Microscopy and Spectroscopy* (Cambridge University Press, Cambridge, 1994).
[26] The code was courteously provided by P. M. Koenraad (COBRA Inter-University Research Institute, Eindhoven University of Technology, The Netherlands), with additions by S. Loth and M. Wenderoth (IV. Physikalisches Institut der Universität Göttingen, Germany).
[27] R. M. Feenstra, J. Vac. Sci. Technol. B **21**, 2080 (2003).
[28] P. Ebert, Appl. Phys. A: Mater. Sci. Process. **75**, 101 (2002).